# Solid-state NMR study of modified clays and polymer/clay nanocomposites

J. GRANDJEAN*

*University of Liege, Institute of Chemistry B6a, COSM, Sart-Tilman, B-4000 Liege, Belgium*

ABSTRACT: Intercalation of surfactant and polymer chains between the clay platelets gives rise to molecular ordering that changes both the chain conformation and mobility with respect to the bulk phase. As a local probe, nuclear magnetic resonance is particularly suited for such investigations, and this review reports the main results obtained in the solid state. The properties of the modified clays are studied as a function of the surfactant loading, the nature of the head group, and the length of the hydrocarbon chain(s). The structure and charge of the mineral also influence the behaviour of molecules in the gallery space. Among papers on polymer/clay nanocomposites, those dealing with poly(ethylene oxide) have been studied in particular, using a multinuclear approach. Natural clays often contain paramagnetic species such as Fe(III) that perturb the nuclear magnetic resonance (NMR) relaxation processes and can prevent observation of appropriate NMR data. Accordingly, most organic/clay hybrids are studied with hectorite or synthetic smectites. However, the paramagnetic effect has also been found useful in characterizing clay dispersion within the polymer matrix of the nanocomposites.

Organo-clay systems are employed in a wide variety of industrial and scientific applications such as adsorbents for organic pollutants (Rheinländer *et al.*, 1998; Meier *et al.*, 2001; Cornejo *et al.*, 2004), pharmaceutical and cosmetic additives (López-Galindo & Viseras, 2004), water treatment (Beall, 2003; Volzone, 2004), catalysts (Meier *et al.*, 2001; Heller-Kallai, 2002; Moronta, 2004), reinforcing fillers for plastics (Wang & Pinnavaia, 1998), rheological control agents (Permien & Lagaly, 1995; Manias *et al.*, 1996), electric (Wu & Lerner, 1993) and nanocomposite materials (Alexandre & Dubois, 2000).

The clayey hybrids are mostly characterized by X-ray diffraction (XRD) and thermogravimetric analysis. For instance, the $d_{001}$ basal spacing from

* E-mail: J.Grandjean@ulg.ac.be

XRD may be related indirectly to the number of surfactant layer(s) and their mean orientation with respect to the clay basal plane (Lagaly, 1986). However, XRD does not describe hybrid materials at a molecular level. Such information is important for understanding the properties of these systems. Vaia *et al.* (1994) used Fourier transform infrared spectroscopy (FTIR) to describe the molecular conformation of alkylammonium salts intercalated in clays. This technique has been applied regularly in the literature as illustrated by more recent data (Li & Ishida, 2003; Zhao *et al.*, 2003). NMR provides a useful technique for characterizing hybrid materials at a molecular level, probing the structure, conformation and dynamics of molecules at inter-faces. The NMR spectroscopy of organo-clay complexes has been reviewed recently (Sanz & Serratosa, 2002; Grandjean, 2004). The NMR information from such clayey systems can be overshadowed by the presence of paramagnetic

ions in the mineral, resulting in the broadening and sometimes disappearance of the NMR lines of nuclei within a few nanometres of the paramagnetic centre. These possible perturbations of the NMR spectra are discussed in the first section of this review. Then a brief account of NMR characterization of the clay inorganic counterions is given, but the main part of this paper concerns NMR data of surfactant and polymer molecules intercalated in phyllosilicates. To obtain clay/polymer nanocomposites, one of the critical steps is the surface treatment of the mineral. Cationic surfactants are often intercalated in clay to ensure its dispersion within the polymer matrix. The local conformation and dynamics of the entrapped molecules determined by NMR provide useful data for understanding the surfactant role in the formation of nanocomposites and the effectiveness of the surface treatment. Different NMR techniques have been proposed to characterize such materials, and they are described briefly below. NMR can obviously be used to show the presence of polymer in the hybrid compounds. However, this review focusses mainly on papers dealing with structural and dynamic information relating to the intercalated organic molecules. The last part of this article summarizes how perturbation of the NMR relaxation processes brought by paramagnetic Fe(III) of natural clays can be used to describe the mineral dispersion in the nanocomposites.

## SOLID-STATE NMR STUDY OF MODIFIED CLAYS

### Magnetism and NMR of clays

In solid materials, the spin (nucleus with a magnetic moment) interactions are anisotropic in nature, resulting often in a broad featureless spectrum. Weak and moderate interactions are cancelled or reduced significantly by spinning the sample at the angle 54.7° (magic angle spinning: MAS) (e.g. Laws *et al.*, 2002; Duer, 2004). The presence of paramagnetic ions, typically $Fe^{3+}$ (Fe(III) to be more precise), in clays such as the widely used montmorillonite must be considered in their NMR studies. A good understanding of the correlations between the magnetism of the mineral and the NMR spectra is a prerequisite for further development of NMR spectroscopy as an efficient tool for studies of clayey materials. Indeed, the magnetic moment of the unpaired electron is approximately three orders of magnitude greater

than that of nuclei, inducing a strong electron-nucleus dipolar interaction, broadening, sometimes beyond the detection limit, the NMR lines and perturbing the NMR relaxation rates within a few nanometres from a given paramagnetic centre. In montmorillonites, paramagnetic Fe(III) atoms substitute partly for Al(III) in the octahedral sheet, giving rise to an electron-nuclear dipolar interaction which becomes the dominant relaxation process for the nearest nuclei. The NMR studies of surfactant-modified clays are summarized in Table 1.

Adapting the equation of the electron-nuclear dipolar Hamiltonian to the $^{13}$C nucleus (equation 1) leads to an interaction frequency as large as 65 kHz.

$$H_D = -\gamma_C \gamma_e \hbar I_z S_{z,n} (3\cos^2\beta_n - 1)/r_n \qquad (1)$$

where $I_z$ is the spin quantum number of the $^{13}$C nucleus, $S_{z,n}$ is the corresponding quantum number of the *n*th electron spin, $r_n$ the distance between the two, and $\beta_n$ is the angle between the external applied magnetic field $B_0$ and the vector $r_n$.

Rapid averaging of the electron spin orientation, brought by the electron spin-electron spin coupling of different Fe(III) atoms (flip-flop term), strongly reduces this interaction as indicated by smaller line-widths of the $^{13}$C NMR spectrum (Yang & Zax, 1999). Fe(III) atom distribution in the octahedral sheet depends drastically on the montmorillonite sample, as shown by Fe EXAFS spectroscopy (Vantelon *et al.*, 2003). Most investigated clays exhibit either a slight or a strong tendency to Fe clustering. In this latter case, the proximity between the paramagnetic sites enhances the electron spin exchange interaction, decreasing the corresponding electronic correlation time in such environment. The Wyoming (Wy-1) montmorillonite (MONT) used most often does not show Fe-Fe pairs. The shortest Fe−Fe distance is ~6.2 Å and, assuming a random distribution of Fe(III), an average distance between two species is calculated to be ~11.4 Å (Yang & Zax, 1999). Furthermore, the composition of naturally occurring clays may be subject to some variations and contain ferromagnetic-like impurities. Recently, measurements of magnetic parameters of three standard clays were performed (Levin *et al.*, 2004): hectorite (HEC), montmorillonite (MONT) (HCa-1 and Wy-1, respectively, from the Source Clays Repository of The Clay Minerals Society, Purdue University, Indiana) and a synthetic mica-montmorillonite SMONT (Barasym SSM-100 from NL Industries). Wy-1 exhibits Langevin paramagnetism with an effective

TABLE 1. Most investigated surfactants.

| Acronym | Cation | Reference |
|---------|--------|-----------|
| BTA | $(CH_3CH_2)_3N^+CH_2C_6H5$ | Bank & Ofori-Oki (1992) |
| DDSA | $(CH_3)_2N^+((CH_2)_{17}CH_3)_2$ | Khatib *et al.* (1996); Osman *et al.* (2002) |
| DDTPP | $(C_6H_5)_3P^+(CH_2)_{11}CH_3$ | Mirau *et al.* (2005) |
| HEDMHA | $(HOCH_2CH_2)N^+(CH_3)_2(CH_2)_{15}CH_3$ | Müller *et al.* (2004) |
| DHEMHA | $(HOCH_2CH_2)_2N^+(CH_3)(CH_2)_{15}CH_3$ | Müller *et al.* (2004) |
| HDTA | $(CH_3)_3N^+(CH_2)_{15}CH_3$ | Pratum (1992); Kubies *et al.* (2002); Müller *et al.* (2004); He *et al.* (2004) |
| HDP | $H_5C_5N^+(CH_2)_{15}CH_3$ | Yei *et al.* (2005) |
| HDTP | $(CH_3)_3P^+(CH_2)_{15}CH_3$ | Hrobarikova *et al.* (2004) |
| HDTBP | $(CH_3(CH_2)_3)_3P^+(CH_2)_{15}CH_3$ | Mirau *et al.* (2005) |
| OA | $H_3N^+(CH_2)_7CH_3$ | Yamauchi *et al.* (2000) |
| ODA | $H_3N^+(CH_2)_{17}CH_3$ | Wang *et al.* (2000); Kubies *et al.* (2002); Osman *et al.* (2004) |
| PA | $H_3N^+(CH_2)_2H_5C_6$ | Bank & Ofori-Oki (1992) |

magnetic moment of 5.5 $\mu_B$ per Fe ion whereas SMONT has diamagnetic properties. At 300 K, the ratio $M/H$ of the bulk dc magnetization ($M$) and the magnetic field ($H$) is larger for HCa-1 (HEC) than that for Wy-1 (MONT) when measurements are made in a magnetic field $H \leqslant 1$ kOe. The opposite is observed in a field of 50 kOe. The difference arises because the magnetization of HCa-1 is dominated by a contribution from ferromagnetic-like impurities while Wy-1 shows paramagnetism. The $^1$H and $^{29}$Si NMR signals of SWy-1 are broadened beyond the detection limit under the experimental conditions used due to the paramagnetic effect (Levin *et al.*, 2004), but increasing the number of scans significantly allows us to observe $^{29}$Si NMR spectra of paramagnetic montmorillonites (Tkáč *et al.*, 1994; Grandjean *et al.*, 2003). By contrast, the HCa-1 yields $^1$H and $^{29}$Si NMR spectra with signal intensities similar to those of the diamagnetic SMONT (Levin *et al.*, 2004). Although it has been shown that the paramagnetic effect may be used to characterize clay dispersion in nanocomposites at low silicate concentration (VanderHart *et al.*, 2001a,b), most NMR studies of modified clay concern synthetic smectites and natural hectorite.

## NMR of inorganic cations in the clay interlayer space

We report only a few recent solid-state NMR data on inorganic ions intercalated between the clay platelets since such studies have been summarized recently both in suspensions (Grandjean, 1998) and in the solid phase (Grandjean, 2004). Interlamellar dipolar nuclei such as $^{113}$Cd exchangeable ions of non (weakly) paramagnetic smectites have been studied by NMR. In HEC with no tetrahedral charge, the hydrated cadmium ions occupy one single site in the centre of the interlayer space along the $c$ axis. A second site in which these ions are displaced closer to the negatively charged basal oxygens is present for montmorillonite (MONT) (Di Leo & Cuadros, 2003). The cation exchange process can be followed by observation of an appropriate nucleus such as $^{23}$Na (Krzaczkowska *et al.*, 2005). Similarly, $^{133}$Cs MAS NMR characterizes the Cs adsorption on the surface of kaolinite and in the interlayer of 2:1 clay minerals, with kaolinite adsorbing less Cs$^+$ than montmorillonite and vermiculite. The first stage of Cs$^+$ adsorption on montmorillonite involves the rapid uptake of cation attachment to the oxygen atoms of the H$_2$O molecules in the interlayer. The second stage arises from a slower cation adsorption to the basal oxygen atoms of the silicate tetrahedral (Ejeckam & Sherriff, 2005). The inter-nuclear dipolar interaction that depends on the nuclear magnetic moments, and the distance and orientation between the nuclei, mediates such transfer of magnetization. Using two dimensional (2D) NMR techniques, structural and interlayer Al ions have been distinguished. Water provides the proton polarization source of the interlamellar ions, and a $^1$H-$^{27}$Al correlation peak occurs at their respective chemical shifts. On the other hand, the structural hydroxyl protons are

correlated with structural Al atoms (Alba *et al.*, 2004). The interaction between the quadrupolar moment $eQ$ of a quadrupolar nucleus ($I > 1/2$) and the electric field gradient, $eq$, generated at the nucleus site by the nuclear environment gives rise to a quadrupolar coupling constant $C_Q$ ($=e^2qQ/h$), splitting the NMR signal. The central line of half-integer spin nuclei is only observed when the quadrupolar splitting exceeds the observable frequency range. When the quadrupolar interaction becomes significant compared to the interaction with the magnetic field (Zeeman interaction), second-order quadrupolar perturbations that are not suppressed by MAS shift and broaden this signal. To obtain high-resolution spectra, appropriate techniques must be used such as two-dimensional multiple quantum magic angle (2D MQMAS) NMR experiments (Rocha *et al.*, 2003; Duer, 2004; Jerschow, 2005). Laponite (LAP), a synthetic hectorite and synthetic saponites (SAP) of variable interlayer charge were characterized by 2D 3QMAS NMR (Delevoye *et al.*, 2003). The clays investigated exhibit only one main contour signal, except for a high-charge saponite (0.75 charge per half unit cell, SAP0.75) where the contour plot is widely distributed in both dimensions. As hydration of kanemite affects the $^{23}$Na 2D 3QMAS NMR spectrum in both dimensions (Hanaya & Harris, 1998), we measured the amount of water in the clay samples by $^1$H NMR, showing similar low contents for the different samples (Delevoye *et al.*, 2003). Although these observations were reproducible,

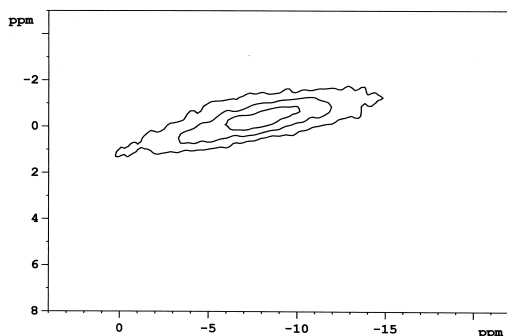more recent saponite samples synthesized with new equipment provide 2D 3QMAS NMR spectra with one single contour plot for saponites of variable interlayer charge (0.35−0.90 charge unit per half-unit cell) (Fig. 1).

Significantly shorter quadrupolar products $P_Q$ ($=C_Q(1+\eta^2/3)^{1/2}$), in the 1.3−1.5 MHz range, are found for the highest-charge clays (SAP0.75, SAP0.80, SAP0.90) compared to 2.1−2.3 for the other saponites (SAP0.35, SAP0.40, SAP0.50, SAP0.60) (Delevoye *et al.*, 2003). Higher symmetry of the counterion environment reduces the electric field gradient and the quadrupolar product (the effect of the asymmetry parameter, $\eta$, varying between 0 and 1 is small). A change to different properties occurs for saponites with an interlayer charge >0.6 per half unit cell. It was shown that such high-charge saponites are characterized by different properties, e.g. the length of the clay particles is multiplied by more than 2 compared to the lower-charge minerals (Michot & Villiéras, 2002). The greater crystallinity of these materials results in a higher ordering process within the gallery space. More order around Na cations gives rise to smaller electric field gradient at the nucleus site. These data suggest one mean interfacial Na$^+$ site for Laponite and all the investigated synthetic saponites. Using similar 2D NMR experiments, hydration of a montmorillonite (MONT) sample with a small Fe(III) content leads to an increase of the quadrupolar product from 1.5 MHz for the dry sample to 3.8 MHz with four water molecules per Na$^+$ ion. This parameter decreases progressively with greater water content to become very small when the hydration structure around Na ions is highly symmetric (octahedral) (Ohkubo *et al.*, 2004).

### NMR of organic species in the clay interlayer space

*Theoretical aspects*. To improve the detection of low-NMR sensitivity nuclei such as $^{13}$C, the polarization of protons can be transferred to these nuclei in the CP experiment. All aspects of dealing with cross-polarization efficiency are reported in a recent paper (Amoureux & Pruski, 2002). During the pulse sequence, the $^{13}$C magnetization $M$ can be approximated by an exponential increase with the time constant $T_{CH}$ whereas the proton magnetization is governed by its relaxation in the rotating frame ($T_{1\rho}(H)$) (Fig. 2).



FIG. 1. $^{23}$Na 2D 3QMAS NMR spectrum of the saponite with 0.75 charge per half unit cell. The projection on the *y* axis (isotropic or high-resolution spectrum) shows a narrow peak, associated with one mean sodium cation environment. The projection on the *x* axis (anisotropic spectrum) provides a much broader signal.
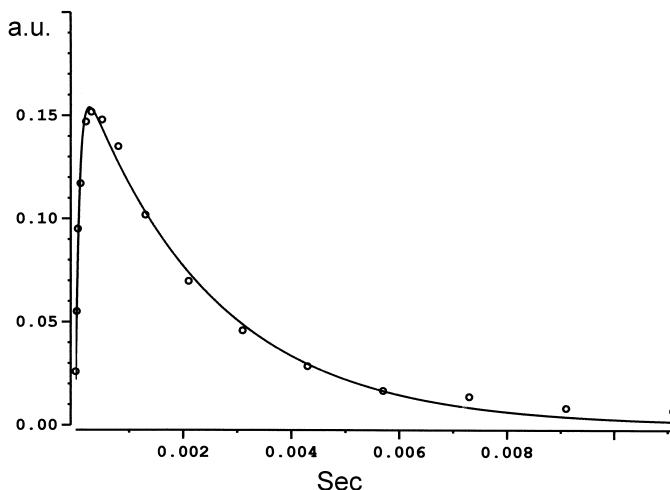
FIG. 2. Plot of the signal intensity as a function of the contact time (LAPDHEMHA: peak at 67.1 ppm)

The variation of the carbon magnetization is ruled by the equation:

$$M(t) = M_0[\exp(-t/T_{1\rho}(H)) - \exp(-t/T_{CH})/[1-T_{CH}(T_{1\rho}(H))^{-1}] \qquad (2)$$

where $t$ is the contact time allowing the polarization transfer from protons to $^{13}$C nuclei and $M_0$ is the equilibrium magnetization. The cross-polarization is most efficient for static $^{13}$C-$^1$H dipolar interaction and mobile groups show greater $T_{CH}$ values. Quantitative data ($M_0$) require spectra to be recorded as a function of the contact time. The assumptions required for application of this equation are described in a review paper (Kolodziejsky & Klinowski, 2002). Quantitative $^{13}$C NMR data can also be obtained by a single pulse experiment that requires a long delay time of ~70 s (five times the relaxation time $T_1$(C)) between two successive pulses. On the other hand, a quantitative CP MAS NMR experiment needs delay times of a few hundreds ms ($5 \times T_{1\rho}(H)$) and the use of typically 15 different contact times. Under appropriate conditions, both experiments on modified clays typically require an overnight run to obtain quantitative data. The CP MAS NMR experiment provides extra information on molecular dynamics from the $T_{CH}$ value variation. Other NMR experiments are also used to probe dynamics of interfacial species in the hybrid compounds. The $T_1$ spin-lattice relaxation times in the laboratory frame are sensitive to molecular motions in the MHz frequency range while the $T_{1\rho}$ relaxation times in the rotating frame and the proton-proton dipolar lineshapes, which can

be measured by using the 2D WISE (WIde line SEparation) NMR experiment, are sensitive to molecular motions on the kHz frequency scale. This last experiment correlates high-resolution $^{13}$C CP MAS NMR frequencies with the low-resolution $^1$H NMR spectrum. The 2D WISE spectrum of the modified clay in which the interlamellar Na cations of SAP0.75 were replaced by hexadecyltrimethyl-ammonium cations (HDTA) is shown (Fig. 3).

The $^{13}$C NMR lines of the hydrocarbon chain are similarly narrow indicating high mobility (Fig. 3, lower) as supported by relaxation data (unpublished results). Broader signals come from motional restriction (Wang *et al.*, 2000; Mirau *et al.*, 2005). Finally, ultraslow dynamics in organically modified clays can be studied by 2D exchange experiments characterized by off-diagonal resonances probing motions on the ms−s timescale (Mirau *et al.*, 2005).

*Applications.* As noted above, NMR studies of organo-clays have been reviewed recently (Sanz & Serratosa, 2002; Grandjean, 2004), and this paper deals with NMR investigations of clay/polymer nanocomposites and their precursors based on surfactant-exchanged smectites. $^{13}$C CP MAS NMR experiments are mostly used to probe the molecular structure and dynamics of organic cations intercalated in phyllosilicates. One of the first studies included the complexes of tetramethyl-ammonium (TMA) and HDTA with MONT and of HDTA with a vermiculite (Pratum, 1992). As the Fe content of these minerals was 3.4 and 7.4%, respectively, the $^{13}$C NMR spectra were poorly resolved, providing two separated signals at ~54
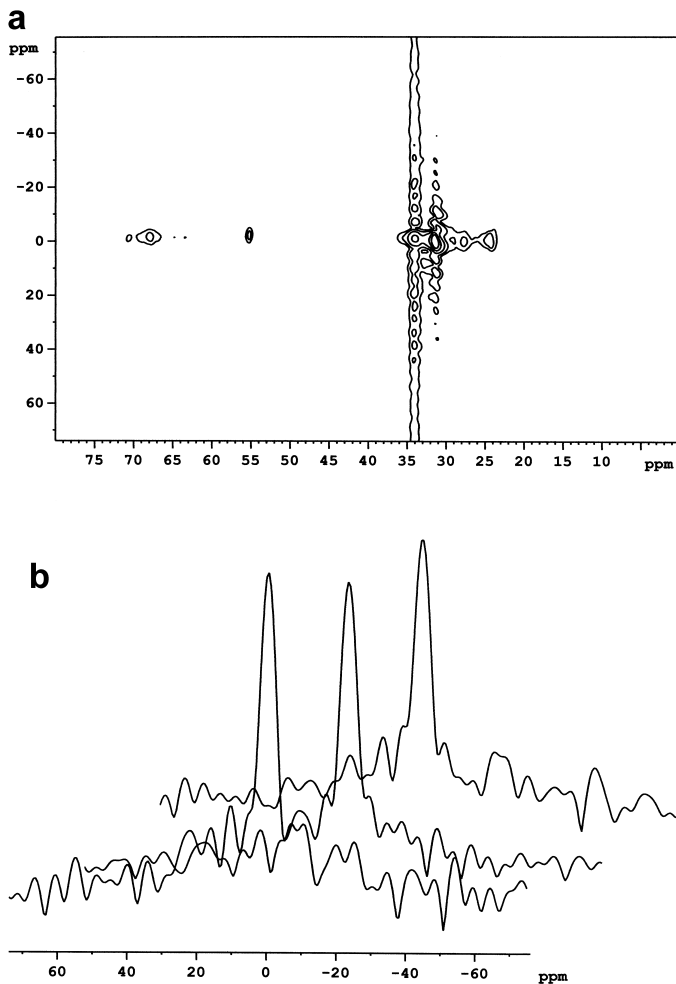
Fig. 3. (a) The $^{13}$C 2D WISE NMR spectrum of HDTASAP0.75 with the $^{13}$C and $^1$H chemical shift scales on the x and y axes, respectively, and (b) the $^1$H projections at the $C_{3,15}$, $NCH_3$ and $C_1$ chemical shifts (from the bottom to the top, respectively).

and 32 ppm assigned to $(CH_3)_3N^+$ and the methylene chain, respectively. Analysis of the relaxation data was hampered by the paramagnetic effect. An increase in the organic cation motion upon intercalation was deduced after subtraction of the estimated paramagnetic relaxation contribution (Pratum, 1992). Bank & Ofori-Oki (1992) assume that the broadening of the aromatic $^{13}$C signals of phenetylammonium (PA) and benzyltriethylammonium (BTA) intercalated in HEC and LAP results from the restriction of the aromatic ring rotation leading to differences in the chemical shifts of the two ortho and the two meta carbons. Physical mixing of the salts and the smectites leads only to a

line broadening with PA, suggesting the role of a proton transfer in this latter case (Bank & Ofori-Oki, 1992). The dipolar constant $T_{CH}$ (equation 2) was measured to describe the variation of the mobility of the methylene groups of dimethyl-distearylammonium (DDSA)-exchanged montmorillonite (DDSAMONT) upon methanol adsorption. The alkyl chains are relatively rigid for alcohol adsorption, typically <0.6 molecules per surfactant head group. Beyond this ratio, the $T_{CH}$ values increase in agreement with mobility enhancement that decreases the dipolar interaction brought by more distant $CH_2$ groups (Khatib et al., 1996). Organic cation mobility was studied by $^1$H NMR in

anhydrous and D$_2$O-saturated TMASAP. $T_1$ proton relaxation time in the laboratory frame of TMA was measured as a function of temperature. Under isotropic rotation diffusion, the $T_1$ plot *vs.* the inverse of temperature (proportional to the correlation time $\tau_c$) shows one minimum. A different plot is obtained for more complex situations. The adapted equation predicts an $\omega^2$ (the frequency $\omega$ is proportional to the external field strength $B_z$) dependence of $T_1$ in the slow-motion domain ($\omega\tau_c \geqslant 1$) whereas a much weaker dependence of $\sim\omega^{1.0}$ was observed below 140 K. The experimental $T_1$ curve as a function of $T^{-1}$ was reproduced by assuming two motional modes: isotropic cation rotation as a whole and translational self-diffusion (Ishimaru *et al.*, 1998). In clay suspensions, $^2$H NMR quadrupolar splitting indicates preferential orientation of molecules and ions near the mineral surface (Grandjean, 1998, 2004). In solids, stronger molecular ordering occurs, resulting in greater line splitting. The apparent $^2$H NMR quadrupolar splitting of ND$_3^+$ in n-octylammonium (OA) ions intercalated in saponite (OASAP) is sensitive to mobility variation (Yamauchi *et al.*, 2000). At 116 K, a splitting of 50 kHz corresponds to the internal rotation of the ND$_3^+$ group of OA around its C$_3$ axis. Cationic uniaxial rotation along the long axis of the intercalated surfactant cation gradually occurs in the 116–400 K temperature range. The non-abrupt reduction of the quadrupolar splitting is also indicative of a wide distribution of the correlation times associated with this rotation. Large-amplitude motion of the whole ion within

the interlayer space accounts for the smaller splitting values obtained at higher temperature. The heterogeneity of the intercalated OA motion could be caused by the inhomogeneous charge distribution in clay layers. These data are supported by $T_1$ measurements as a function of the correlation time (Yamauchi *et al.*, 2000).

In the solid state, the conformation of long-chain surfactant is all-*trans* as indicated by one single $^{13}$C NMR signal near 34 ppm, assigned to the internal methylene groups of the alkyl chain. After intercalation between the clay platelets, this signal is split. The higher field component at ~31 ppm results from the so-called $\gamma$ *gauche* effect providing an upfield shift for the $\gamma$ carbon in the *gauche* conformation. Higher temperatures lead to the decrease of the all-*trans* conformation (Fig. 4).

Such a conformational heterogeneity was observed by $^{13}$C CP MAS NMR techniques in MONT exchanged with octadecylammonium (ODA) cations. The $T_{CH}$ values (equation 2) of the 34 and 31 ppm signals suggest that molecules in the ordered all-*trans* conformation are as rigid as those in the solid crystalline materials whereas the molecules in the disordered conformation are similar to those of liquid crystalline materials. Upon heating, the molecules in the ordered conformation become disordered. However, the ODA ions intercalated in MONT never attained the complete liquid-like behaviour even in the disordered conformation (Wang *et al.*, 2000). The Li ions of a partially delaminated mica were exchanged with dialkyldimethylammonium cations,
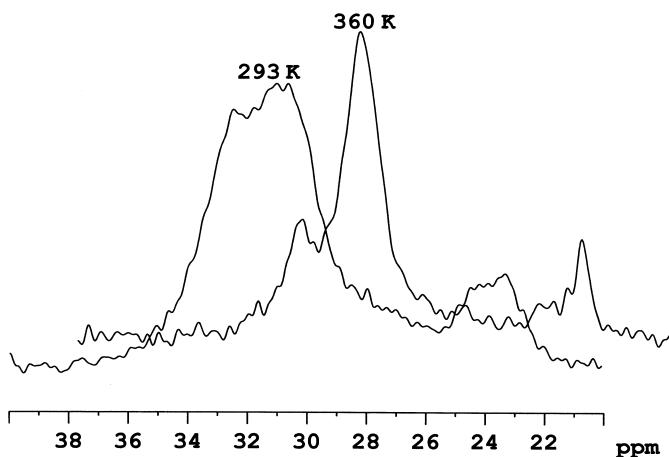


Fig. 4. $^{13}$C CP MAS NMR spectra of the main CH$_2$ signals of HDTA intercalated in LAP at 293 and 360 K. The scale of the higher-temperature spectrum is shifted to the right by 2.5 ppm.

varying the alkyl tail from $C_{12}$ to $C_{18}$. At $-25°C$, a single line is observed at 33 ppm, characteristic of the all-*trans* conformation of the hydrocarbon chain. With increasing temperature, a second resonance at ~30 ppm grows in while the intensity at 33 ppm decreases, indicating the formation of a dynamic average between the *gauche* and *trans* conformations. The time scale for a molecule to move between the ordered and disordered phase was estimated as being slower than 1 s from 2D exchange spectra. The conformational change was fully reversible (Osman *et al.*, 2002). All-*trans* and *gauche* conformations coexist also for HDTA and ODA intercalated in LAP (LAPHDTA and LAPODA). In contrast with MONTODA, a lower percentage of the all-*trans* conformer (40% instead of 80%) and higher surfactant mobility were measured in LAPODA. For instance, the $^{13}C$ relaxation time in the laboratory frame increases regularly from $C_1$ to $C_{16}$ as observed in the fast motion limit ($\omega\tau_c \ll 1$). The smaller size, the structural difference of LAP platelets and the different arrangement (monolayer instead of bilayer) of the intercalated surfactant can account for such a different behaviour (Kubies *et al.*, 2002). A single layer of intercalated cations in LAPHDTA, parallel to the silicate surface, is consistent with the low clay charge of LAP, implying weak surfactant content after the 1/1 exchange. The ammonium cations are individually separated; therefore, the interchain interactions are weak. This dilution effect causes the formation of *gauche* conformer; meanwhile, the hydrocarbon tails that are parallel to the silicate layers have a full contact with the silicate surface. The repulsive forces from the silicate surface increase the mobility of the hydrocarbon chain and therefore result in high concentrations of *gauche* conformer (Li & Ishida, 2003). Synthetic saponites of variable charge were modified by exchanging the original Na cations with HDTA (1/1 exchange). For the two lowest-charge saponites, the surfactant cations adopt a bilayer structure with long alkyl chains lying down on the clay surface. The increase of the clay charge (and the surfactant loading) leads to variation of the hydrocarbon tail orientation from parallel to radiating away from the silicate surface, forming the so-called paraffin complex with the highest-charge minerals. The all-*trans* conformation of the intercalated surfactant also fluctuates with the saponite charge. From being dominant for the lowest charges, it reaches a minimum value for intermediate charges and then

evolves progressively to the highest all-*trans* conformation population with the mineral charge (Fig. 5). Similar observations were observed after intercalation of (hydroxyethyl)dimethylhexadecyl-ammonium (HEDMHA) or (dihydroxyethyl)methyl-hexadecylammonium (DHEMHA), changing the head group (Müller *et al.*, 2004). Under the 1/1 cation exchange used to obtain the modified saponites, high charge also means high surfactant loading. A few months later, a similar observation was reported for MONTHDTA, varying the surfactant loading between 0.2 and 5 times the cation exchange capacity (CEC) of MONT (He *et al.*, 2004). Both sets of data with SAP and MONT can be explained similarly, resulting from the interplay between the repulsive silicate surface−hydrocarbon chain interaction, and the inter-chain van der Waals interactions between the hydrogen atoms that increase with the surfactant concentration, favouring the all-*trans* conformation of the alkyl chains. Until near the minimum, the alkyl chains remain approximately parallel to the silicate surface, whereas they radiate away from the clay surface for higher surfactant loadings. This results from the increase of the interchain interactions that favour the all-*trans* configuration, forming paraffin-type monolayer and paraffin-type bilayers for the highest clay contents (Müller *et al.*, 2004; He *et al.*, 2004). Fourier transform infrared (FTIR) data suggest also that the interaction between the head group and the clay surface influence the ordering of the hydrocarbon tail: strong ion-ion interaction resulting in more disordered conformation than weak ion-dipole interaction (Li & Ishida, 2003). The $^{13}C$ MAS NMR results are not only complementary to that of
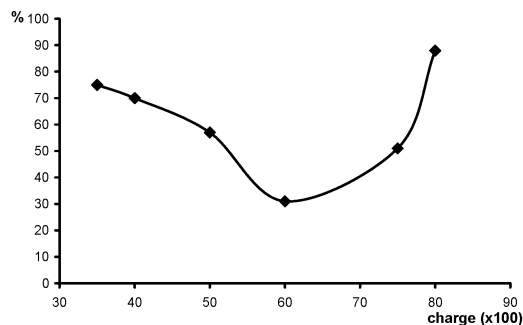
FIG. 5. All-*trans* conformer population (%) of HDTA main alkyl chain as a function of the saponite charge ($10^2$) per half unit cell.

FTIR data but also provide new insights into the conformational ordering of the intercalated surfactants (He *et al.*, 2004). Furthermore, only NMR spectroscopy is able to estimate unambiguously the all-*trans* conformational content of differently charged systems (Müller *et al.*, 2004). Measurement of the dipolar time constant $T_{CH}$ (equation 2) supports the greater rigidity of the all-*trans* conformation and the decrease of the head group mobility after substitution of methyl group(s) by hydroxyethyl chain(s). This latter effect may be associated with the interaction of the hydroxyl group with the silicate layer but no NMR or IR data support this assumption. Therefore, a steric effect might be considered (Müller *et al.*, 2004). The $^{13}$C $T_1$ relaxation times for the organically-modified clays are substantially shorter than those of the semi-crystalline surfactant, supporting fast molecular motions on a MHz frequency scale that are not present in the bulk surfactant (Kubies *et al.*, 2002; Müller *et al.*, 2004). Mono-(1ODA), di-(2ODA), tri-(3ODA), and tetra-octadecylammomium (4ODA) cations were also intercalated in MONT. The $^{13}$C MAS NMR spectra of the modified clays were recorded in the temperature range of −19 to +65°C. On going from MONT4ODA to MONT1ODA, the available space per alkyl chain increases, leading to less ordering and line broadening. MONT1ODA did not show any temperature dependence. In contrast to MONT3ODA and MONT4ODA in which the all-*trans* conformation of the alkyl chain is only present at −19°C, *gauche* segments do exist in MONT2ODA, indicating less order and looser packing. The increase of the averaged *gauche*/*trans* to all-*trans* ratio with temperature in MONT2-4ODA suggests an order-disorder transition. The coexistence of ordered and disordered segments below and above the phase transition is indicated by its spreading over a temperature range (Osman *et al.*, 2004). The mobility of the head group of the phosphonium salts can be probed by the relaxation time measurements of the highly NMR sensitive $^{31}$P nucleus. Thus, Laponite and synthetic saponites were cation-exchanged with the bromide of hexadecyltrimethylphosphonium (HDTP). The *trans*/*gauche* conformational ratios were similar to those obtained previously for the intercalated ammonium cations (Kubies *et al.*, 2002; Müller *et al.*, 2004). Greater head group mobility was observed for LAPHDTP, as a result of the weakest electrostatic interaction of the organic

cation with this octahedrally substituted clay. Motional restriction, increasing with the clay charge, was observed for the modified saponites (Hrobarikova *et al.*, 2004). Different $^{31}$P NMR techniques were also performed to study the mobility of hexadecyltributylphosphonium (HDTBP) and dodecyltriphenylphosphonium (DDTPP) intercalated in Laponite. In the proton dimension of the 2D WISE NMR experiments ($^{13}$P-$^1$H correlation), the line widths of LAPDDTPP are twice as large as for LAPHDTBP, indicating that of the DDTPP are more restricted on the 50 kHz frequency scale. Varying the mixing time in the 2D exchange pulse sequence results in the $^{31}$P nucleus reorientation on a time scale of 1 s (Mirau *et al.*, 2005). Hexadecylpyridinium cations (HDP) and its inclusion complex in α-cyclodextrin were intercalated in MONT. The $^{13}$C CP MAS NMR spectrum of the latter material was indeed similar to the spectrum of the pure inclusion complex (Yei *et al.*, 2005).

During the synthesis of hectorite by hydrothermal crystallization of magnesium silicate, tetraethylammonium (TEA) ions were used to aid crystallization and became progressively incorporated as the exchange cations within the interlayer. $^{13}$C NMR shows evidence of TEA-clay formation in as little as 30 min and also that 80% of the final TEA loading is accomplished in the first 10−12 h. Up to 36 h more are needed to incorporate the remaining 20% of TEA. Accordingly, initial nucleation and crystallization end after ~14 h, after which primary agglomeration of particles takes place (Carrado *et al.*, 2000).

### SOLID-STATE NMR STUDY OF POLYMER/CLAY NANOCOMPOSITES

#### Structure and dynamics

Composites of polymers with smectite clay minerals have received significant attention because of improvements in mechanical, thermal and barrier properties that can result from synergistic effects of the polymer and the lamellar solid (Alexandre & Dubois, 2000). Such materials which usually contain a few percent of clay can be prepared by different methods, depending on the polymer properties. The interlayer gap can be swelled using long-chain alkyl amine or ammonium salts, easing the intercalation of the polymer. The

polymer precursor can be intercalated between the clay platelets and can then be converted to the final polymer by appropriate chemical processes. Nanocomposites containing polymers may still be obtained by using the *in situ* intercalative polymerization approach: the monomer is first intercalated and appropriate treatment leads to polymerization in the interlayer space. Nanocomposites can be also formed by mixing the polymer and the layered silicate together and heating the mixture above the glass transition of the polymer. Finally, the polymer may aid the nucleation and growth of the inorganic host crystals and get trapped within the layers as they grow (Alexandre & Dubois, 2000). The bulk organization of these materials is usually described as phase separated, intercalated or exfoliated systems, depending on the mineral dispersion within the polymer matrix. The NMR studies of polymer/clay nanocomposites are summarized in Table 2.

Polymer chains surround stacked clay platelets in microcomposites. Intercalated nanocomposites contain polymer chains at least partly inserted in the clay galleries and exfoliated nanocomposites refer to systems with single clay platelets dispersed within the polymer matrix.

Acrylamide intercalated in kaolinite (KAO) was polymerized (PAAM) *in situ*. The polymerization, which was completed after 1 h of treatment was followed by the change of the $^{13}C$ signal intensity of the ethylenic carbon atoms (Sugahara *et al.*, 1990). Polymerization of ethylene glycol intercalated in kaolinite was not observed. However, poly(ethylene glycol)(PEG)/KAO intercalates were obtained by mixing dimethylsulphoxide/KAO complexes and polymer (melt) at 150–200°C, partially releasing dimethylsulphoxide from KAO. $^{13}C$ MAS techniques suggest more constrained polymer mobility in the interlamellar space of the mineral than in its bulk (Tunney & Detellier, 1996).

Poly(ethylene oxide) (PEO) complexes are interesting materials due to their anisotropic ionic conductivity. Intercalation of PEO in clay results in a nanocomposite polymer electrolyte potentially useful for solid-state secondary batteries. Solid-state high-resolution NMR was applied to study (PEO)/hectorite samples. The $^{13}C$ CP MAS NMR spectrum of pure PEO shows two signals at 70.6 and 71.9 ppm, respectively. For crystalline PEO, with a helicoidal structure presenting only *gauche* $CH_2-CH_2$ conformation, the spectrum is expected to give a single signal near 70 ppm. The second signal is assigned to the interaction between different chains in the solid state or the presence of some methylene groups in the *trans* conformation. Intercalation of PEO in $Na^+$-, $K^+$- or $Ba^{2+}$-hectorite leads to a single peak close to 70 ppm, attributed to a *gauche* conformation of the

TABLE 2. Most investigated polymers.

| Acronym | Cation | Reference |
|---|---|---|
| NY-6 | $(HN(CH_2)_6NHCO(CH_2)_4CO)_n$ | Usuki *et al.* (1995); Mathias *et al.* (1999); VandenHart *et al.* (2001a,b,c) |
| P2Epy | $(CH_2CH(C_5H_5N^+H))_n$ | Sahoo *et al.* (2003) |
| PAAM | $(CH_2CH(CONH_2))_n$ | Sugahara *et al.* (1990) |
| PAN | $(CH_2CH(CN))_n$ | Bourbigot *et al.* (2004) |
| PANI | $(C_6H_4NH)_n$ | Goddard *et al.* (2003) |
| PCL | $(OCO(CH_2)_5)_n$ | Hrobarikova *et al.* (2004); Calberg *et al.* (2004); Krzaczkowska *et al.* (2005) |
| PEO (PEG) | $(CH_2\text{-}CH_2\text{-}O)_n$ | Aranda & Ruiz-Hitzky (1992); Tunney & Detellier (1996); Wong *et al.* (1996); Wong & Zax (1997); Yang & Zax (1999); Harris *et al.* (1999); Kwiatkowski & Whittaker (2001); Hou *et al.* (2002, 2003); Lorthioir *et al.* (2005) |
| PGLU | $(HNCH((CH_2)_2COOH)CO)_n$ | Gougeon *et al.* (2003) |
| PLYS | $(HNCH((CH_2)_4NH_2)CO)_n$ | Gougeon *et al.* (2002, 2003) |
| PMMA | $(CH_2C(CH_3)(COOCH_3))_n$ | Chen *et al.* (2002); Forte *et al.* (1998) |
| PS | $(CH_2CH(C_6H_5))_n$ | Hou *et al.* (2003); Bourbigot *et al.* (2003, 2004); Hou & Schmidt-Rohr (2003); Yang & Zax (2006) |
| PVA | $(CH_2CHOH)_n$ | Asano *et al.* (2004) |

methylene groups, suggesting that the helical conformation is maintained in the nanocomposite (Aranda & Ruiz-Hitzky, 1992). The small chemical shift variations found for intercalation compounds containing different interlayer cations could be associated with interactions between the oxyethylene units of the polymer and those interlayer cations. Such cation-polymer interaction was revealed by $^{23}Na$ NMR spectroscopy. The composite materials show a peak at $-10.8$ ppm, whereas the $^{23}Na$ NMR spectrum of dry HEC shows two signals at $-21.6$ and $-30.6$ ppm resulting from interaction of Na ions with the silicate oxygen atoms. With 50% relative humidity, a broad signal with several peaks was observed. Thus, the intercalation of PEO leads to an increase in the homogeneity of the Na environment and simultaneously to a decrease of $Na^+$ interactions with the silicate oxygens (Aranda & Ruiz-Hitzky, 1992). Numerous (2D) solid-state NMR techniques are currently used to describe the structure and dynamics of solids (Duer, 2004). Such an experiment was performed to estimate the extent of the *gauche* conformation in PEO-based materials. $Na^+$-HEC and PEO with 13% $^{13}C$-$^{13}C$ labelled units in stoichiometric amounts were stirred in acetonitrile for 24 h to obtain the relevant nanocomposite. Using a two-dimensional (2D) NMR techniques, the OC–CO bonds were found to be 90±5% *gauche* (Harris *et al.*, 1999), supporting the previous investigations (Aranda & Ruiz-Hitzky, 1992). The PEO/HEC nanocomposite was used to optimize the conditions of several 2D NMR experiments dedicated for studying organic species near silicate surface. As the internuclear dipolar interaction depends on the distance between the nuclei, its time-modulation allows us to estimate the latter parameter. Thus, the protons of the polymer closest to the clay surface are a distance of $2-4$ Å from the structural OH groups of HEC (Hou *et al.*, 2002). $^2H$ NMR was used to study dynamics of deuterated PEO intercalated in $Li^+$-fluorohectorite. Although the spectrum of the bulk polymer reveals no significant dynamics at 220 K, small-amplitude motions of PEO are present in the composite materials. Increasing temperature up to 400 K gives rise to a gradual onset of polymer dynamics. The anisotropic pattern of the spectrum disappears when all orientations are equally probable, giving the single line spectrum of the isotropic phase (melt phase). Unlike in the bulk, significant anisotropic features persist in the $^2H$ NMR spectrum of the nanocomposite at temperatures well above the melting temperature of the polymer. This indicates that many polymer units are trapped between silicate layers and are preferentially oriented with respect to the surrounding silicate structure (Wong *et al.*, 1996; Yang & Zax, 2006). 2D $^2H$ exchange spectroscopy allows us to study C-H dynamics on the ms timescale. Above the $T_g$ of PEO, large-angle reorientation is observed for the bulk polymer but not in the intercalated nanocomposite sample. The best simulation of the 2D spectrum for inserted PEO indicated reorientation of the C-$^2H$ bond vectors through angles somewhat <30°, and through some mix of sloppy jumps with limited rotational diffusion which cover the full range of orientation in a few ms of evolution (Yang & Zax, 2006).

Relaxation rates $R_1$ in the laboratory frame are sensitive to fluctuations in the local environment on a timescale comparable to the inverse of the NMR resonance frequency (i.e. nanoseconds). At low temperature, relaxation rates are greater in the intercalated sample, corresponding to greater polymer mobility than that in the bulk phase (Wong *et al.*, 1996). Accordingly, the $^7Li$ NMR spectra of PEO/$Li^+$-HEC at high temperatures indicate that cation reorientation, like polymer reorientation, is somewhat less than isotropic, and residual ordering is imposed by the long parallel plates of the silicate lattice. The deviation of the cation surrounding distribution of oxygen atoms from tetrahedral implies greater quadrupolar interactions, not totally cancelled at high temperatures (Wong *et al.*, 1996). Compared to the PEO/$Li^+$-HEC sample, extra broadening of the $^7Li$ NMR signal occurs with PEO/$Li^+$MONT(Wy-1) samples due to the presence of $Fe^{3+}$ in the octahedral layer of the smectite. Each $Fe^{3+}$ contributes an unpaired electron, forming a magnetic field roughly 1000 times as large as that of a typical nuclear spin. The electron spins undergo rapid spin flips, and the effective coupling (line width) to the nuclei is proportional to the inverse of temperature, as is the case for internuclear coupling. Such a variation of the $^7Li$ NMR line width of PEO/$Li^+$- MONT is indeed observed at high (>300 K, internuclear couplings dominate) and low temperatures (<250 K). At intermediate temperatures, however, the line shape narrowing is much more dramatic. We interpret this transition region as the temperature range over which $Li^+$ dynamics are capable of averaging the electron spin coupling to the nuclear

spin. It is estimated that the correlation time for the Li$^+$ hopping is a hundred-fold greater than the correlation time for polymer reorientation. Thus, lineshape-narrowing studies in the presence of fixed paramagnetic sites is a measure of cation dynamics. Cation dynamics in these nanocomposites is approximately two orders of magnitude slower than polymer reorientation (Wong *et al.*, 1996; Wong & Zax, 1997). Simulation of $^7$Li NMR spectra indicates that cations interact with the silicate surface layer and their diffusion is restricted to the surface (Yang & Zax, 1999). Recently, it has been established that $^7$Li NMR shows that the nearest neighbour hydration state of Li$^+$ is unaffected by PEO intercalation in MONT (Wy-1 and synthetic) (Reinholdt *et al.*, 2005). By contrast, $^{23}$Na NMR indicates that PEO insertion results in the conversion of the multiple Na$^+$ hydration states into inner sphere sites probably likely formed through coordination with the silicate oxygens. This tighter binding of Na$^+$ to the clay may be the origin of the conductivity of PEO/Na$^+$-MONT being slower by two orders of magnitude than that of PEO/Li$^+$-MONT. The results confirm the idea that polymer oxygen atoms do not participate in sequestering the exchangeable cations and agree with a jump process for cation migration (Reinholdt *et al.*, 2005).

Nanocomposites were also prepared by melt intercalation of PEO into synthetic montmorillonite. The $^1$H and $^{13}$C relaxation rates were measured as a function of temperature. There was no observed change in the rates at the transition temperature expected for pure PEO, progressively decreasing temperature. Therefore, large-amplitude motion of the intercalated polymer chains persist below the glass transition of the pure macromolecule. The similarities between the $^{13}$C CP MAS spectra of PEO and PEO/MONT suggest that the conformation and type of motion within the two systems are similar and consist of helical jumps but the jump motion in the nanocomposite has a lower apparent activation energy (Kwiatkowski & Whittaker, 2001).

Melt intercalation was also used to obtain poly(styrene-ethylene oxide) block copolymers(PS-*b*-PEO)/HEC materials, starting with a clay/block copolymer mixture (4/1). Polymer intercalation was assessed by 2D $^1$H-$^{29}$Si, $^1$H-$^{13}$C heteronuclear and $^1$H-$^1$H homonuclear correlation spectra. $^1$H and $^{13}$C nuclei of intercalated molecules are close to $^{29}$Si nuclei and structural hydroxyl protons of HEC. The proximity of two spin-1/2 nuclei may induce specific signal enhancements, resulting from the modulation of the dipolar interaction (Duer, 2004). Two polymers with similar PEO block lengths (7 and 8.4 kDa) but different PS block lengths (3.6 *vs.* 30 kDa) were compared. While the PS blocks are found not to be intercalated in either material, PEO intercalation does occur with the shorter PS block length. In the PS-rich sample, a significant fraction of PEO is not intercalated, however (Hou *et al.*, 2003). Similar techniques were used more recently to characterize PEO/LAP (1/1) systems, suggesting interactions between PEO chains and Laponite layers. Proton relaxation decay in the laboratory frame is bi-exponential, indicating two domains: PEO chains intercalated in LAP and a PEO phase containing clay platelets, probably in the exfoliated state. With the PEO/LAP (3/7) nanocomposite, the first domain is only present and the blend is homogeneous on a length scale of ~10 nm (Lorthioir *et al.*, 2005).

2D $^2$H exchange spectroscopy was also used to investigate PS incorporated in modified fluorohectorite. Above the $T_g$ of PS, reorientation angles up to ~45° are accessed *via* small-angle diffusive hops. By contrast, there is no evidence for slow dynamics at the backbone sites in the bulk phase (Yang & Zax, 2006).

$^1$H-$^{27}$Al heteronuclear correlation NMR spectra were recorded to characterize the organic-inorganic interfacial structure of polylysine (PLYS) in synthetic montmorillonite and beidellite. The results indicate that the ammonium protons of the positively charged lateral chains are located near the silicate layer, at a distance <0.6 nm, indicating that polylysine side chains are intercalated between the clay platelets (Gougeon *et al.*, 2002). The chemical shifts of the $^{13}$C CP MAS NMR spectra reflect an overall loss of helicity of polylysine intercalated in MONT, and the adoption of a single, more extended conformation. A similar but less important effect is also observed with polyglutamic acid (PGLU). Unlike PLYS, the side chains do not have any positive charges, therefore, to overcome the repulsion from the negative charges of the clay, carboxylic groups are protonated. This explains the different structures in the interlayer region between PLYS and PGLU (Gougeon *et al.*, 2003). More recent studies indicate reduced local mobility of positively charged side chains of PLYS, suggesting their penetration within the interlayer space and their interaction with the negatively charged clay layers (Gougeon *et al.*, 2006).

Mixing of 2-ethynylpyridine and dried MONT in benzene at 65°C for 24 h gives hybrid materials the solid-state $^{13}$C CP MAS NMR spectra of which prove the formation of poly(2-ethynylpyridine) (P2Epy) within the lamellar galleries of MONT as a result of *in situ* polymerization. At a lower adsorption yield (8%), the polymer is more tightly bound to the clay surface (shorter dipolar relaxation time $T_{CH}$, equation 2), and as the adsorption yield (15−22%) increases, the fraction of the loosely bound polymer increases. Variation of the $^{13}$C NMR signal frequency as a function of the polymer yield and protonation of the intercalated polymer indicates partial neutralization of the positive charge on the nitrogen of the intercalated polymer by its interaction with the negative charge of the mineral (Sahoo *et al.*, 2003).

No known solvent is capable of dispersing hydrophyllic unmodified clays and dissolving hydrophobic polymers simultaneously. Therefore, the mineral is organically modified, exchanging the original inorganic cations with cationic surfactants, protonated monomers or positively charged polymer initiators. Thus, anilinium cations were first intercalated in montmorillonite and polymerized to give a polyaniline (PANI)/clay nanocomposite. Among the different oxidation states of this conducting polymer, the most investigated forms are emeraldine (EB, insulator) in which the reduced and oxidized units are equal, and emeraldine salt (ES) which shows idealized structures of the protonated form due to proton doping. $^{2}$H static and MAS NMR studies reveal similar spectral features for EB and PANI/MONT whereas a Knight

shift observed with ES suggests that polarons are involved in charge transport. Failure to detect a Knight shift in PANI/MONT is consistent with the importance of 3D mechanisms of charge transfer for bulk conductivity in PANI, not possible in the nanocomposite (Goddard *et al.*, 2003). The gel polymer electrolyte based on poly(methylmethacrylate) (PMMA) has also been proposed for Li battery application, particularly because of their beneficial effects on the stabilization of the Li-electrolyte interface. The corresponding nanocomposites were prepared by *in situ* polymerization of methylmethacrylate (MMA), in the presence of organomodified MONT. The carboxyl and methylene chemical shifts of PMMA are not influenced by the presence of MONT. Upon Li$^{+}$ addition, two minor shoulders appear downfield which become more intense with the clay content. Therefore, the clay mineral promotes the basicity of the carboxyl groups enhancing the interaction with Li cations. However, the balanced attractive forces among silicate layers, carboxyl groups, Li cations and anions is critical in order to result in greater ionic conductivity (Chen *et al.*, 2002).

Intercalated nanocomposites with a high clay content were prepared by the *in situ* polymerization of ε-caprolactone in the presence of modified saponites of variable interlayer charge. Typical $^{13}$C CP MAS NMR spectra are shown in Fig. 6 for the modified saponite HDTASAP0.75 and the corresponding nanocomposite. The signals of the bottom spectrum are assigned to N-CH$_2$ (68 ppm), NCH$_3$ (54 ppm), H$_2$C$_{4-14}$ in the all-*trans* conformation (34 ppm), H$_2$C$_{4-14}$ in the dynamically
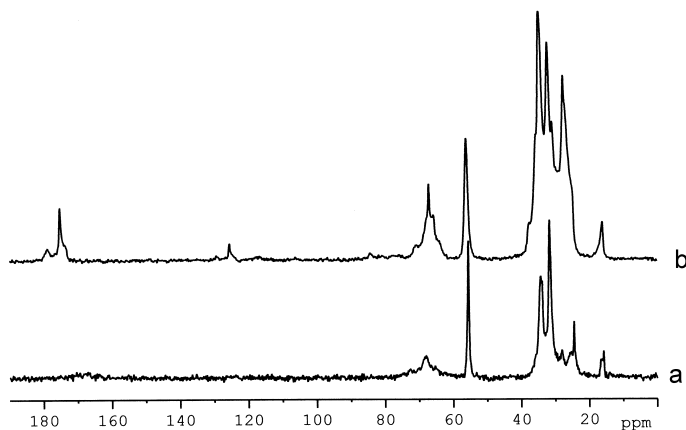


FIG. 6. $^{13}$C CP MAS NMR spectrum of HDTASAP0.75 (a) and PCL/HDTASAP0.75 (b), showing both the HDTA and PCL resonances (polymer content: 25%)

exchanged *trans/gauche* conformation (32 ppm), $H_2C_2$ (29 ppm), $H_2C_{3,15}$ (25 ppm) and the terminal $H_3C_{16}$ group (17 ppm), respectively (Kubies *et al.*, 2002).

The polymer peaks of the nanocomposite are readily attributed to the O-CO (174 ppm,) O-CH$_2$ (66 ppm), CO-CH$_2$ (34 ppm), OC-CH$_2$-CH$_2$ (30 ppm) and the two remaining methylene groups (26 ppm) (the signal at 125 ppm is a spinning side band). Such hybrid materials allow us to determine the *trans/gauche* conformational ratio of the surfactant hydrocarbon chain and to characterize the surfactant (HDTA) (Kubies *et al.*, 2002; Müller *et al.*, 2004; Mirau *et al.*, 2005), and poly(ε-caprolactone) (PCL) ($M_w \sim 4$ kDa) mobility in the nanocomposites. The decrease of the *trans* conformer population in the HDTA (HDTP) hydrocarbon chain and the variation of the $^{31}$P relaxation times of the intercalated HDTP show the presence of greater mobility after nanocomposite formation as also deduced from the $^{13}$C CP MAS NMR spectra (equation 2) The dipolar relaxation times $T_{CH}$ (equation 2), shorter in the extracted PCL than that in the nanocomposite, indicate greater polymer mobility in the nanocomposite than in the bulk phase, as also observed upon surfactant intercalation. No significant effect on the structure and dynamics of these intercalated nanocomposites was observed by varying the layer charge of the starting saponites, although the clay charge can affect the yield of the prepared nanocomposite (Hrobarikova *et al.*, 2004). The yields of PCL intercalation were weaker with surfactant-exchanged Laponites than with similarly modified synthetic saponites, as a result of unavoidable polymer-clay interactions that appear in the first system. The small platelet size of LAP may also affect the polymer intercalation process. PCL motion, occurring mainly in the kHz range, decreases from the centre to the end of the monomer unit (Urbanczyk *et al.*, 2006).

Copolymers of MMA and 2-(methyl-N,N-diethylammoniumiodide) ethylacrylate (MDEA) inserted in bentonite and hectorite were prepared in two different ways. The clay was first functionalized by exchange with MDEA and MMA was then allowed to copolymerize with the modified mineral. The second type of complex was obtained by direct interaction of the preformed copolymers with the smectite. The comparison between the $^{13}$C $T_1$ relaxation times of the pure copolymers with the HEC complexed ones shows only minor differences

and no dependence on the preparation method or on the MMA/MDEA ratio. The $^{13}$C relaxation times in the rotating frame that are sensitive to slower motions in the kHz range are significantly different for the complex prepared by the first method, suggesting a different structure of the copolymer in this material. In the paramagnetic bentonite samples, the relaxation times are shorter for all the investigated systems, indicating proximity of the clay layers containing paramagnetic Fe(III) atoms and the copolymer molecules through the $R_4N^+$ group. This observation also supports polymer intercalation in bentonite. Furthermore, cross-polarization is inefficient for the $^{13}$C nuclei close to the paramagnetic centres due to the drastic shortening of $T_{1\rho}(H)$ (equation 2). The paramagnetic effect is weaker with the materials prepared with the functionalized bentonites. It is proposed that a small percentage of MMA copolymerizes with MDEA thus forming a small MDEA/MMA ratio copolymer, while a large part of MMA forms essentially long MMA sequences which are attached to the clay through an MDEA moiety, but mainly outside of the layers (Forte *et al.*, 1998).

The first polymer-clay nanocomposite based on nylon 6, described in the early 1990s, was prepared by polymer insertion in surfactant-exchanged montmorillonites (typically 5%). In particular, $^{15}$N CP MAS NMR study of model hybrid compounds indicates a strong interaction with the silicate layers. It was suggested that montmorillonite interacts strongly with the ammonium end groups of nylon 6 (NY-6), with the polymer chains perpendicular to the clay surface (Usuki *et al.*, 1995). This technique was also applied to characterize the different phases of this polymer in the hybrid material. The α-crystalline (thermodynamically favoured) and amorphous phases are usually only observed in the pure polymer. An extra signal, assigned to the γ crystal form, with an intensity similar to that of the α phase was observed in the nanocomposite spectrum. Annealing of the hybrid material under conditions that produce α crystallinity in neat nylon 6, results in the γ crystal form and amorphous phases. It was concluded that the protonated amine end groups are tightly bonded to the clay surface, giving rise to an alignment of the polymer chains parallel to each other, an appropriate orientation for formation of the γ crystalline phase, but not of the layered hydrogen-bonded sheets leading to the α form (Mathias *et al.*, 1999). Several nominally 95/5 NY-6/MONT nanocomposites made by melt blending or *in situ*

polymerization were studied by the $^{13}C$ CP MAS NMR technique. The resonances at 34 ppm and 26.3 ppm are convenient indicators of the γ- and α-forms, respectively. The presence of the clay promotes the formation of the γ phase of NY-6. The relative contributions of both forms upon different technical treatments were estimated similarly (VanderHart *et al.*, 2001a).

### Clay dispersion and paramagnetic relaxation.

The quality of the clay dispersion is a key factor in the preparation of the nanocomposite. Transmission electron microscopy (TEM) and X-ray diffraction (XRD) are generally used for that purpose. The Fe(III) paramagnetic content of natural montmorillonites can enhance drastically the $^{1}H$ and $^{13}C$ spin-lattice relaxation rates of the polymer nuclei. The paramagnetic contribution $(T_1(H)^{para})$ to $T_1(H)$ is approximated as:

$$(T_1(H)^{para})^{-1} \equiv$$
$$R \approx (T_1(H))^{-1} - (T_1(H)^{NY-6})^{-1} \qquad (3)$$

with $(T_1(H)^{NY-6})$ the $T_1(H)$ of the pure polymer. Clay layers having no polymer interfaces, by and large do not influence $T_1(H)$, and their paramagnetic effect is indeed the most efficient when the smectite is fully exfoliated. For families of nanocomposites with the same clays (i.e. the same $Fe^{3+}$ concentration in each clay layer) and the same NY-6/MONT stoichiometry, $T_1(H)^{para}$ (and $T_1(H)$) was found to be correlated with the quality of the clay dispersion (VanderHart *et al.*, 2001b,c). With some *in situ* polymerized samples, annealing gives rise to decreasing of the α/γ phase ratio. Because the mere presence of the clay is sufficient to change the dominant crystal form of NY-6 from α to γ, it could be anticipated that the γ phase would be nucleated mainly near the clay surface. That the $^{1}H$ relaxation rate in the γ crystallites is faster than that of the α crystallites supports this assumption since shorter proton−clay surface distances increase the paramagnetic effect and the observed relaxation rate $1/T_1(H)$ (VanderHart *et al.*, 2001b). With the clay modifiers used to obtain some melt blending nanocomposites, narrow proton resonances occur on the top of the $^{1}H$ broad lineshape of NY-6 in the hybrid material. The relative signal intensities and the chemical shifts indicate the formation of amino compounds of small size, resulting from the modifier degradation. The combination of temperature and mechanical stresses, rather than just

temperature itself, was the principal cause of the chemical degradation of the modifier (VanderHart *et al.*, 2001b,c).

Similar modified montmorillonites with two slightly different $Fe_2O_3$ concentrations were used to prepare nanocomposites by melt blending of poly(ε-caprolactone) (PCL) or by *in situ* polymerization of ε-caprolactone. Variation of $(T_1(H)^{para})^{-1}$ (equation 3) as a function of the clay content is shown in Fig. 7 for the nanocomposites obtained by melt intercalation. As expected, this parameter increases with the clay content, and significant differences in the $(T_1(H)^{para})^{-1}$ values between the two clays are shown even at a clay content as low as 1%.

Clustering of clay platelets (microcomposites), decreasing the paramagnetic effect on the relaxation process, should lead to a progressive levelling of the curve. The opposite is observed, indicating no important clay aggregation until a mineral content of 50%. PCL/MONT nanocomposites prepared by *in situ* polymerization gave rise either to intercalated nanocomposites similar to those obtained by melt blending or exfoliated nanocomposites. At the same clay content, the latter samples induce a stronger paramagnetic effect than the former as might have been predicted. However, no correlation between nanocomposites prepared by *in situ* polymerization and melt blending was found. The $^{13}C$ relaxation time in the rotating frame $T_{1\rho}(C)$ was also used to describe polymer dynamics of these polymer-rich materials which remain similar for clay contents in the 0−30% range, showing greater mobility in the middle of the monomer chain (Calberg *et al.*, 2004).
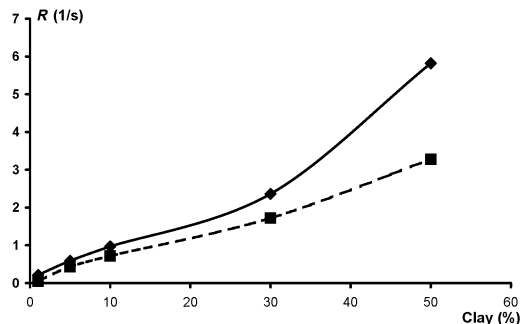


FIG. 7. Paramagnetic contribution $R$ (s$^{-1}$) (equation 3) as a function of clay content (■ $Fe_2O_3$: 3.41%; ◆ $Fe_2O_3$: 3.51%) (reprinted with permission from Calberg *et al.*, 2004; Copyright (2004) American Chemical Society).

Poly(vinyl alcohol) (PVA)/montmorillonite nano-composites form well-exfoliated systems. To show how the polymer $T_1(H)$ values depend on the amount of $Fe^{3+}$, a few nanocomposites were prepared with three montmorillonites sharing different $Fe^{3+}$. A good relation between the paramagnetic contribution factor to $T_1(H)$ and the $Fe_2O_3$ content suggests that the latter can be estimated by just measuring $T_1(H)$ (Asano *et al.*, 2004). In the light of a non-NMR paper (Vantelon *et al.*, 2003), such a correlation is not expected to be general but dependent on the possible $Fe^{3+}$ aggregation within the clay layer (Calberg *et al.*, 2004).

[1]H spin-lattice relaxation decay curves of paramagnetic nanocomposites were also analysed by separation in two regions: a narrow and a much broader region experiencing direct and indirect paramagnetically induced relaxation, respectively. The former region, in the 5−50 ms range, was used to calculate the fraction *f* of the actual polymer-clay interfacial area, relative to the maximum possible polymer-clay interfacial area. The decay at longer times was associated with the degree of homo-geneity, ε, of the distribution of the polymer-clay surfaces. Data analysis was performed for several deoxygenated PS/MONT nanocomposites. The aromatic polymers indeed cause a major shortening of $T_1(H)$) because oxygen has specific interactions with aromatic rings. Good correlation was found with XRD and TEM data; however, there are cases in which serious questions about the representative character of high-magnification images available arise. The morphology of these hybrid materials changes from microcomposite to exfoliated nano-composite, depending on the preparation procedure. Analysis of samples equilibrated with atmospheric oxygen can provide quick but less quantitative information on clay dispersion within the polymer matrix (Bourbigot *et al.*, 2003). That approach was later applied to styrene-acrylonitrile copolymer nanocomposites for systems showing an intercalated structure with some exfoliation and the presence of small tactoids, whatever the loading in MONT was. The polymer-clay interfacial area, *f*, was estimated at 0.5 and the degree of homogeneity characterizing the distribution of MONT platelets is ~40% (Bourbigot *et al.*, 2004).

The previous NMR studies on dia- or para-magnetic nanocomposites were synthesized after clay modification. An alternate procedure, based on micellar systems was also proposed. By sonification of unmodified HEC dispersed in water and surfactant micellized polymer in toluene, PS-clay intercalated nanocomposites were prepared. The previously cited [1]H-[29]Si and [1]H-^{1}H correlation solid-state NMR experiments show that the HDTA protons are the closest to the clay surface. These nanocomposites consist of ~50 nm diameter stacks of intercalated clays dispersed in the polystyrene matrix, forming a layer of ~20 nm around the clay stack (Hou & Schmidt-Rohr, 2003).

# CONCLUSIONS

Solid-state NMR is an emerging technique in the study of the structure and dynamics of species intercalated in clay. In surfactant-exchanged clays, the main results concern modulation of the all-*trans* conformation upon variation of the clay structure, the mineral charge, the surfactant loading or the temperature. These results not only complement FTIR data but also provide new insights into the conformational ordering of the intercalated surfac-tants. Furthermore, application of NMR techniques is more general. Arrangement of polymer chains in the clay galleries can be also described by NMR methods. NMR spectroscopy is also useful in studying molecular dynamics. Thus, the mobility of intercalated surfactant depends on its arrange-ment and conformation in the interlayer region. Variation of the polymer chain motion upon nanocomposite formation can also be characterized by NMR methods. At this stage, no general rule can be defined since quite different systems showing sometimes opposite effects have been reported. The NMR methods are also quite useful in describing the structure of the polymer in the hybrid material and its intercalation extent.

Most of the above studies have been performed with synthetic clays and hectorite which are devoid of paramagnetic effects perturbing the NMR data. Nevertheless, this destructive perturbation has been used to define clay dispersion within the polymer matrix of nanocomposites.

REFERENCES

Alba M.D., Castro M.A., Naranjo M. & Perdigón A.C. (2004) Structural localization of $Al^{3+}$ ions in aluminosilicates: application to heteronuclear chemical shift correlation to 2:1 silicates. *Physics and Chemistry of Minerals*, **31**, 195−202.

Alexandre M. & Dubois P. (2000) Polymer-layered silicate nanocomposites: preparation, properties and uses of a new class of materials. *Materials Science and Engineering*, **28**, 1−63.

Amoureux J.-P. & Pruski M. (2002) Theoretical and experimental assessment of single- and multiple-quantum polarization in solid-state NMR. *Molecular Physics*, **100**, 1595−1613.

Aranda P. & Ruiz-Hitzky E. (1992) Poly(ethylene oxide)/silicate intercalation materials. *Chemistry of Materials*, **4**, 1395−1403.

Asano A., Shimizu M. & Kurotsu T. (2004) Effect of paramagnetic $Fe^{3+}$ on $T_1{}^H$ in PVA/montmorillonite-clay nanocomposites. *Chemistry Letters*, **33**, 816−817.

Bank S. & Ofori-Oki G. (1992) Solid-state reaction of phenethylammonium chloride and Al-exchanged clays as followed by cross-polarization/magic angle spinning nuclear magnetic resonance spectroscopy. *Langmuir*, **8**, 1688−1689.

Beall G.W. (2003) The use of organo-clay in water treatment. *Applied Clay Science*, **24**, 11−20.

Bourbigot S., VanderHart D.L., Gilman J.W., Awad W.H., Davis R.D., Morgan A.B. & Wilkie C.A. (2003) Investigation of nanodispersion in polystyrene-montmorillonite nanocomposites by solid-state NMR. *Journal of Polymer Science: Part B: Polymer Physics*, **41**, 3188−3213.

Bourbigot S., VanderHart D.L., Gilman J.W., Ballayer S., Stretz H. & Paul D.R. (2004) Solid-state NMR characterization and flammability of styrene-acrylonitrile copolymer montmorillonite nanocomposite. *Polymer*, **45**, 7627−7638.

Calberg C., Jérôme R. & Grandjean J. (2004) Solid-state NMR study of poly(ε-caprolactone)/clay nanocomposites. *Langmuir*, **20**, 2039−2041.

Carrado K.A., Xu L., Gregory D.M., Song K., Seifert S. & Botto R.E. (2000) Crystallization of a layered silicate clay as monitored by small-angle X-ray scattering and NMR. *Chemistry of Materials*, **12**, 3052−3059.

Chen H.-W., Lin T.-P. & Chang F.-C. (2002) Ionic conductivity enhancement of the plasticized PMMA/$LiClO_4$ polymer nanocomposite electrolyte containing clay. *Polymer*, **43**, 5281−5288.

Cornejo J., Celis R., Cox L. & Hermosin M.C. (2004) Pesticide-clay interactions and formulations. Pp. 247−266 in: *Clay Surfaces: Fundamentals and Applications* (E. Wypych & K.G. Satyanarayana, editors). Elsevier, Amsterdam, The Netherlands.

Delevoye L., Robert J.-L. & Grandjean J. (2003) $^{23}Na$ 2D 3QMAS NMR and $^{29}Si$, $^{27}Al$ MAS NMR investigation of Laponite and synthetic saponites of variable interlayer charge. *Clay Minerals*, **38**, 63−69.

Di Leo P. & Cuadros J. (2003) $^{113}Cd$, $^1H$ MAS NMR and FTIR analysis of $Cd^+$ adsorption on dioctahedral and trioctahedral smectites. *Clays and Clay Minerals*, **51**, 403−414.

Duer M.J. (2004) *Introduction to Solid-state NMR Spectroscopy*. Blackwell Science, Oxford, UK.

Ejeckam R.B. & Sherriff B.L. (2005) A $^{133}Cs$, $^{29}Si$, and $^{27}Al$ MAS NMR spectroscopic study of Cs adsorption by clay minerals: Implications for the disposal of nuclear wastes. *The Canadian Mineralogist*, **43**, 1131−1140.

Forte C., Geppi M., Giamberini S., Giacomo R., Veracini A. & Mendez B. (1998) Structure determination of clay/methymethacrylate copolymer interlayer complexes by means of $^{13}C$ solid-state NMR. *Polymer*, **39**, 2651−2656.

Goddard Y.A., Vold R.L. & Hoatson G.L. (2003) Deuteron NMR study of polyaniline and polyaniline/clay nanocomposite. *Macromolecules*, **36**, 1162−1169.

Gougeon R.D., Rheinholdt M., Delmotte L., Miehé-Brendlé J., Chézeau J.-M., Le Dred R., Marchal R. & Jeandet P. (2002) Direct observation of polylysine side-chain interaction with smectites interlayer surfaces through $^1H$-$^{27}Al$ heteronuclear correlation NMR spectroscopy. *Langmuir*, **18**, 3396−3398.

Gougeon R.D., Rheinholdt M., Delmotte L., Miehé-Brendlé J., Chézeau J.-M., Le Dred R., Marchal R. & Jeandet P. (2003) Polypeptide adsorption on a synthetic montmorillonite: A combined solid-state NMR spectroscopy, X-ray diffraction, thermal analysis and $N_2$ adsorption study. *European Journal of Inorganic Chemistry*, 1366−1372.

Gougeon R.D., Rheinholdt M., Delmotte L., Miehé-Brendlé J., Chézeau J. & Jeandet P. (2006) Solid-state NMR investigation on the interactions between a synthetic montmorillonite and two homopolypeptides. *Solid State Nuclear Magnetic Resonance*, **29**, 322−329.

Grandjean J. (1998) NMR studies of interfacial phenomena. *Annual Reports on NMR Spectroscopy*, **35**, 217−260.

Grandjean J. (2004) NMR spectroscopy of molecules and ions at clay surfaces. Pp. 216−246 in: *Clay Surfaces: Fundamentals and Applications* (E. Wypych & K.G. Satyanarayana, editors). Elsevier, Amsterdam, The Netherlands.

Grandjean J., Bujdák J. & Komadel P. (2003) NMR study of surfactant molecules intercalated in montmorillonite and in silylated montmorillonite. *Clay Minerals*, **38**, 367−373.

Hanaya M. & Harris R.K. (1998) Two-dimensional $^{23}Na$

MQ MAS NMR study of layered silicates. *Journal of Material Chemistry*, **8**, 1073–1079.

Harris D.J., Bonagamba T.J. & Schmidt-Rohr K. (1999) Conformation of poly(ethylene oxide) intercalates in clay and MoS$_2$ studied by two-dimensional double-quantum NMR. *Macromolecules*, **32**, 6718–6724.

He H., Frost R.L., Deng F., Zhu J., Wen X. & Yuan P. (2004) Conformation of surfactant molecules in the interlayer of montmorillonite, studied by $^{13}$C MAS NMR. *Clays and Clay Minerals*, **52**, 350–356.

Heller-Kallai L. (2002) Clay catalysis in reactions of organic matter. Pp. 567–614 in: *Organo-Clay Complexes and Interactions* (S. Yariv & H. Cross, editors). Marcel Dekker Inc., New York, USA.

Hou S.S. & Schmidt-Rohr K. (2003) Polymer-clay nanocomposites from directly micellized polymer/toluene in water and their characterization by WAXD and solid-state NMR spectroscopy. *Chemistry of Materials*, **15**, 1938–1940.

Hou S.S, Beyer F.L. & Schmidt-Rohr K. (2002) High-sensitivity multinuclear NMR spectroscopy of a smectite clay and clay-intercalated polymer. *Solid State Nuclear Magnetic Resonance*, **22**, 110–127.

Hou S.S., Bonagamba T.J., Beyer F.L., Madison P.H. & Schmidt-Rohr K. (2003) Clay intercalation of poly(styrene-ethylene oxide) block copolymers studied by two-dimensional solid-state NMR. *Macromolecules*, **36**, 2769–2776.

Hrobarikova J., Robert J.-L., Calberg C., Jérôme R. & Grandjean J. (2004) Solid-state NMR study of intercalated species in poly(ε-caprolactone)/clay nanocomposites. *Langmuir*, **20**, 9828–9833.

Ishimaru S., Yamauchi M. & Ikeda R. (1998) Dynamics of interlayer cations in tetramethylammonium-saponite studied by $^1$H, $^2$H NMR and electrical conductivity measurements. *Zeitschrift für Naturforschung*, **53a**, 903–908.

Jerschow A. (2005) From nuclear structure to quadrupolar NMR interaction and high-resolution spectroscopy. *Progress in Nuclear Magnetic Resonance Spectroscopy*, **46**, 63–78.

Khatib K., François M., Tekely P., Michot L.J., Bottero J.Y. & Baudin I. (1996) Immersion microcalorimetry and $^{13}$C CP MAS NMR study of the structure of organoclays. *Journal of Colloids and Interface Science*, **183**, 148–154.

Kolodziejski W. & Klinowski J. (2002) Kinetics of cross-polarization in solid-state NMR: A guide for chemists. *Chemical Reviews*, **102**, 613–628.

Krzaczkowska J., Fojud Z., Kozak M. & Jurga S. (2005) Spectroscopic studies of poly(ε-caprolactone)/sodium montmorillonite nanocomposites. *Acta Physica Polonica A*, **108**, 187–196.

Kubies D., Jérôme R. & Grandjean J. (2002) Surfactant molecules intercalated in Laponite as studied by $^{13}$C and $^{29}$Si MAS NMR. *Langmuir*, **18**, 6159–6163.

Kwiatkowski J. & Whittaker A.K. (2001) Molecular motion in nanocomposites of poly(ethylene oxide) and montmorillonite. *Journal of Polymer Science: Part B: Polymer Physics*, **39**, 1678–1685.

Lagaly G. (1986) Interaction of alkylamines with different types of layered compounds. *Solid State Ionics*, **22**, 43–51.

Laws D.D., Bitter H.-M. & Jerschow A. (2002) Solid-state NMR spectroscopic methods in chemistry. *Angewandte Chemie International Edition*, **41**, 3096–3129.

Levin E.M., Hou S.-S., Bud'ko S.L. & Schmidt-Rohr K. (2004) Magnetism and nuclear magnetic resonance of hectorite and montmorillonite layered silicates. *Journal of Applied Physics*, **96**, 5085–5092.

Li Y. & Ishida H. (2003) Characterization-dependent conformation of alkyl tail in the nanoconfined space: Hexadecylamine in the silicate galleries. *Langmuir*, **19**, 2479–2484.

López-Galindo A. & Viseras C. (2004) Pharmaceutical and cosmetic applications of clays. Pp. 267–279 in: *Clay Surfaces: Fundamentals and Applications* (E. Wypych & K.G. Satyanarayana, editors). Elsevier, Amsterdam, The Netherlands.

Lorthioir C., Sulpice-Gaillet C., Lauprêtre F., Soulestin J., Gloaguen J.-M. & Lefebvre J.-M. (2005) Bulk organization and chain dynamics in poly(ethylene oxide)/Laponite and poly(methyl methacrylate)/poly(ethylene oxide)/Laponite nanocomposites: Solid-state NMR investigations. *8$^{th}$ European Symposium on Polymer Blends and Eurofillers 2005 (Joint Meeting)*, Bruges, Belgium.

Manias E., Hadziionnanou G. & Brinke G. (1996) Inhomogeneities in sheared ultra thin lubricating films. *Langmuir*, **12**, 4587–4593.

Mathias L.J., Davis R.D. & Jarrett W.L. (1999) Observation of α and γ crystal forms and amorphous regions of nylon-6 clay nanocomposites using solid-state $^{15}$N nuclear magnetic resonance. *Macromolecules*, **32**, 7958–7960.

Meier L.P., Nueesch R. & Madsen F.T. (2001) Organic pillared clays. *Journal of Colloid and Interface Science*, **238**, 24–32.

Michot L.J. & Villiéras F. (2002) Assessment of surface energetic heterogeneity of synthetic Na-saponites. The role of the clay charge. *Clay Minerals*, **37**, 39–57.

Mirau P.A., Vaia R.A. & Garber J. (2005) NMR characterization of the structure and dynamics of polymer interfaces in clay nanocomposites. *Polymer Preprints*, **46**, 440–441.

Moronta A. (2004) Catalytic and adsorption properties in modified clay surfaces. Pp. 321–344 in: *Clay Surfaces: Fundamentals and Applications* (E. Wypych & K.G. Satyanarayana, editors). Elsevier, Amsterdam, The Netherlands.

Müller R., Hrobarikova J., Calberg C., Jérôme R. &

Grandjean J. (2004) Structure and dynamics of cationic surfactants intercalated in synthetic clays. *Langmuir*, **20**, 2982−2985.

Ohkubo T., Saito K., Kanehashi K. & Ikeda Y. (2004) A study on hydration behaviours of interlayer cations in montmorillonite by solid-state NMR. *Science and Technology of Advanced Materials*, **5**, 693−696.

Osman M.A., Ernst M., Meier B.H. & Suter U.W. (2002) Structure and molecular dynamics of alkane monolayers self-assembled on mica platelets. *Journal of Physical Chemistry B*, **106**, 653−662.

Osman M.A., Ploetze M. & Skrabal P. (2004) Structure and properties of alkylammonium monolayers self-assembled on montmorillonite platelets. *Journal of Physical Chemistry B*, **108**, 2580−2588.

Permien T. & Lagaly G. (1995) The rheological and colloidal properties of bentonites dispersions in the presence of organic compounds V. Bentonite and sodium montmorillonite and surfactants. *Clays and Clay Minerals*, **43**, 229−236.

Pratum T.K. (1992) A solid-state $^{13}$C NMR study of tetraalkylammonium/clay complexes. *Journal of Physical Chemistry*, **96**, 4567−4571.

Reinholdt M.X., Kirkpatrick R.J. & Pinnavaia T.J. (2005) Montmorillonite-poly(ethylene oxide) nanocomposites: Interlayer alkali metal behaviour. *Journal of Physical Chemistry B*, **109**, 16296−16303.

Rheinländer T., Klumpp E. & Schwuger M.J. (1998) On the adsorption of hydrophobic pollutants on surfactant/clay complexes: comparison of the influence of a cationic and a non-ionic surfactant. *Journal of Dispersion Science and Technology*, **19**, 379−398.

Rocha J., Morais C.M. & Fernandez C. (2003) Novel nuclear magnetic resonance techniques for the study of quadrupolar nuclei in clays and other layered materials. *Clay Minerals*, **38**, 259−278.

Sahoo S.K., Kim D.W., Kumar J., Blumstein A. & Cholli A.L. (2003) Nanocomposite from in-situ polymerization of substituted polyacetylene within the lamellar surface of the montmorillonite: A solid-state NMR study. *Macromolecules*, **36**, 2777−2784.

Sanz J. & Serratosa J.M. (2002) NMR spectroscopy of organo-clay complexes. Pp. 223−272 in: *Organo-Clay Complexes and Interactions* (S. Yariv & H. Cross, editors). Marcel Dekker Inc., New York, USA.

Sugahara Y., Satokawa S., Kuroda K. & Kato C. (1990) Preparation of a kaolinite-polyacrylamide intercalation compound. *Clays and Clay Minerals*, **38**, 137−143.

Tkáč I., Komadel P. & Müller D. (1994) Acid-treated montmorillonites − A study by $^{29}$Si and $^{27}$Al MAS NMR. *Clay Minerals*, **29**, 11−19.

Tunney J.J. & Detellier C. (1996) Aluminosilicate nanocomposite materials. Poly(ethylene glycol) kaolinite intercalates. *Chemistry of Materials*, **8**, 927−935.

Urbanczyk L., Hrobarikova J., Robert J.-L., Calberg C., Jérôme R. & Grandjean J. (2006) Motional heterogeneity of intercalated species in modified clays and poly(ε-caprolactone)/clay nanocomposites. *Langmuir*, **22**, 4818−4824.

Usuki A., Kojima Y., Kawasumi M., Okada A., Kurauchi T. & Kamigaito O. (1995) Interaction of nylon 6 − clay surface and mechanical properties of nylon 6 hybrid. *Journal of Applied Chemistry*, **55**, 119−123.

Vaia R.A., Teukolsky R.K. & Giannelis E.P. (1994) Interlayer structure and molecular environment of alkylammonium layered silicates. *Chemistry of Materials*, **6**, 1017−1022.

VanderHart D.L., Asano A. & Gilman J.W. (2001a) Solid-state NMR investigation of paramagnetic nylon-6 clay nanocomposites 1. Crystallinity, Morphology, and the direct influence of $Fe^{3+}$ on nuclear spins. *Chemistry of Materials*, **13**, 3781−3795.

VanderHart D.L., Asano A. & Gilman J.W. (2001b) Solid-state NMR investigation of paramagnetic nylon-6 clay nanocomposites 2. Measurement of clay dispersion, crystal stratification, and stability of organic modifiers. *Chemistry of Materials*, **13**, 3796−3809.

VanderHart D.L., Asano A. & Gilman J.W. (2001c) NMR measurements related to the clay-dispersion quality and organic-modifier stability in nylon-6/clay nanocomposites. *Macromolecules*, **34**, 3819−3822.

Vantelon D., Montarges-Pelletier E., Michot L.J., Briois V., Pelletier M. & Thomas F. (2003) Iron distribution in the octahedral sheet of dioctahedral smectites. An Fe K-edge X-ray absorption spectroscopy study. *Physics and Chemistry of Minerals*, **30**, 44−53.

Volzone C. (2004) Removal of metals by naturals and modified clays. Pp. 290−320 in: *Clay Surfaces: Fundamentals and Applications* (E. Wypych & K.G. Satyanarayana, editors). Elsevier, Amsterdam, The Netherlands.

Wang L.-Q., Liu J., Exarhos G.J., Flanigan K.Y. & Bordia R. (2000) Conformational heterogeneity and mobility of surfactant molecules in intercalated clay minerals studied by solid-state NMR. *Journal of Physical Chemistry B*, **104**, 2810−2816.

Wang Z. & Pinnavaia T.J. (1998) Nanolayer reinforcement of elastomeric polyurethane. *Chemistry of Materials*, **10**, 3769−3771.

Wong S. & Zax D.B. (1997) What do NMR line widths tell us? Dynamics of alkali cations in a PEO-based nanocomposite polymer electrolyte. *Electrochimica Acta*, **42**, 3513−3518.

Wong S., Vaia R.A., Giannelis E.P. & Zax D.B. (1996) Dynamics in poly(ethylene oxide)-based nanocomposite polymer electrolyte probed by solid state NMR. *Solid State Ionics*, **86-88**, 547−557.

Wu J.H. & Lerner M.M. (1993) Structural, thermal, and electrical characterization of layered nanocomposites derived from Na-montmorillonite and polyethers. *Chemistry of Materials*, **5**, 835−838.

Yamauchi M., Ishimaru S. & Ikeda R. (2000) Dynamics of n-octylammonium ions intercalated in saponite. *Molecular Crystals and Liquid Crystals*, **341**, 315−320.

Yang D.-K. & Zax D.B. (1999) Li^{+} dynamics in polymer nanocomposite: An analysis of dynamic line shapes in nuclear magnetic resonance. *Journal of Chemical Physics*, **110**, 5325−5336.

Yang D.-K. & Zax D.B. (2006) Multidimensional ^{2}H NMR study of dynamical heterogeneity in polymer nanocomposites. *Solid State Nuclear Magnetic Resonance*, **29**, 153−162.

Yei D.-R., Kuo S.-W., Fu H.-K. & Chang F.-C. (2005) Enhanced thermal properties of PS nanocomposites formed from montmorillonite treated with a surfactant/cyclodextrin inclusion complex. *Polymer*, **46**, 741−750.

Zhao Z., Tang T., Qin Y. & Huang B. (2003) Relationship between the continually expanded interlayer distance of layered silicates and excess intercalation of cationic surfactants. *Langmuir*, **19**, 9260−9265.